

## A MINI-SURVEY OF X-RAY POINT SOURCES IN STARBURST AND NON-STARBURST GALAXIES

R. E. KILGARD, P. KAARET, M. I. KRAUSS, A. H. PRESTWICH, M. T. RALEY, A. ZEZAS

Harvard-Smithsonian Center for Astrophysics, Cambridge, MA 02138

*Draft version November 8, 2018*

## ABSTRACT

We present a comparison of X-ray point source luminosity functions of 3 starburst galaxies (the Antennae, M82, and NGC 253) and 4 non-starburst spiral galaxies (NGC 3184, NGC 1291, M83, and IC 5332). We find that the luminosity functions of the starbursts are flatter than those of the spiral galaxies; the starbursts have relatively more sources at high luminosities. This trend extends to early-type galaxies which have steeper luminosity functions than spirals. We show that the luminosity function slope is correlated with  $60\mu\text{m}$  luminosity, a measure of star formation. We suggest that the difference in luminosity functions is related to the age of the X-ray binary populations and present a simple model which highlights how the shape of the luminosity distribution is affected by the age of the underlying X-ray binary population.

*Subject headings:* surveys — galaxies: spiral — galaxies: starburst — X-rays: galaxies — X-rays: sources

## 1. INTRODUCTION

The study of X-ray point source populations in external galaxies may permit insights into the evolution of various stellar populations within galaxies (Fabbiano 1989). Since most luminous X-ray point sources are related to objects produced at the end-point of the evolution of massive stars, the population of bright X-ray point sources should be related to the history of massive star formation. With the recent launch of the Chandra and XMM-Newton X-ray observatories, we can finally study the X-ray point source populations in a sample of galaxies with a variety of star formation histories with high angular resolution and good sensitivity. This may permit insights into the relation of the X-ray point source populations to the stellar evolutionary history of each galaxy.

There is evidence to suggest that galaxies with high star formation rates contain a greater number of ultra-luminous X-ray sources ( $L_x > 10^{39} \text{ erg s}^{-1}$ ). For example, there are several such sources in each of the starburst galaxies M82 (Zezas et al. 2001), the Antennae (Fabbiano et al. 2001), NGC 3256 (Lira et al. 2001). By contrast, none are found in the non-starburst/normal spiral galaxies IC 5332 or NGC 3184 (see Fig. 1). However, several biases must be considered that could affect such “anecdotal” evidence. More massive galaxies may have more ultra-luminous X-ray sources because there is a greater likelihood of finding rare sources in larger systems. Nearby galaxies (e.g. Local Group galaxies) have such large angular extents that Chandra surveys have been incomplete, and sources in unexplored regions may have been missed. The most important biases are probably source confusion and higher source detection thresholds in more distant galaxies.

Here we study the X-ray point source luminosity functions (LFs) in a “mini-survey” of Chandra observations of four spiral and three starburst galaxies. Our sample covers a range of Hubble types and concentrates on nearby galaxies to reduce problems with confusion and incompleteness. We describe our sample of galaxies and data analysis procedures in §2. Our results on the X-ray luminosity functions are presented in §3 and compared with previous results in §4. In §5, we describe a simple model which attempts to relate the luminosity function to the age of the X-ray binary population in each galaxy. We present our conclusions in §6.

## 2. SAMPLE SELECTION AND DATA ANALYSIS

We chose a sample of nearby galaxies representing many different Hubble types in an attempt to reduce the intrinsic biases and study the dependence of the LF parameters on star formation activity. For the spirals, we selected relatively nearby galaxies with favorable inclinations in order to minimize problems with source confusion, incompleteness, and obscuration. We obtained new Chandra observations for NGC 1291 and IC 5332 and used archival data for NGC 3184 and M83. An analysis of NGC 1291 has also been presented by Irwin et al. (2001). The paucity of nearby starbursts forces us to relax our standards. We selected the two nearby starbursts with available Chandra data M82 (Griffiths et al. 2001; Zezas et al. 2001; Ward et al., in preparation) and NGC 253 (Strickland et al. 2000). To increase the sample, we also include the more distant Antennae galaxies (Fabbiano et al. 2001; Zezas and Fabbiano 2001). More than 70% of the  $D_{25}$  ellipse of each galaxy, except one, was in the Chandra field of view. The exception was NGC 253 where the field of view covered only 45% of the  $D_{25}$  ellipse, but did include the entire starburst region.

We note that M83 has a starburst in the nuclear and bar region (e.g. Telesco et al. (1993)), but the star formation rate is low compared to classic starbursts (Rieke and Lebofsky 1978) and confined to a small part of the galaxy. Most of our detected X-ray sources are outside the starburst region (approximately 30 arcsecs around the nucleus; Alton et al. (1998)) and are representative of the disk population rather than the starburst population. M83 is probably best characterized, in general, as a composite object. However, our luminosity function for this galaxy is dominated by the disk population and we group it together with the spirals. The  $60\mu\text{m}$  luminosity plotted in figure 2 is an upper limit to the luminosity from the area over which we detect the most X-ray sources.

Observations of all galaxies (except M82) were performed on the back-illuminated ACIS-S3 CCD. M82 was observed on the ACIS-I3 front-illuminated CCD, which has lower sensitivity below 2 keV than ACIS-S3. However, the difference in sensitivity is not significant compared with the uncertainties in distances and assumed source spectra.

All analyses were performed using the Chandra Interactive Analysis of Observations software package (*CIAO*) v2.1.2 and

the Chandra Calibration Database v2.6. Data were screened for times of high background, as many of the observations occurred near periods of solar activity. Exposure times of the screened observations are in Table 1. Source lists were constructed using *wavdetect* (Freeman et al. 2002), the Mexican-hat wavelet source detection routine which is part of *CIAO*. We ran *wavdetect* on 0.3-6.5 keV band images using wavelet scales of 2, 4, 8, and 16 pixels. This combination of energy band and wavelet scales yielded the fewest spurious detections and found all visually obvious point sources. The output source regions were visually inspected to remove the artifacts that sometimes occur with *wavdetect*: regions where the ellipse minor axis is zero, regions containing 2 sources, and sources detected twice. Nuclear sources, when present, were removed from the source lists, as were sources outside the  $D_{25}$  ellipses.

Source regions were taken to be 4 times the standard deviation of the distribution. This over-estimates the source size, but the contribution from background is negligible. For each source, PHA spectra were extracted and RMFs and ARFs were constructed. Corresponding background spectra were extracted for each source. The region for each background spectrum was taken to be an ellipse with radii equal to 4 times the source radii and excluding the source regions and any other overlapping source regions. To limit contamination from any diffuse emission, the background ellipse radii were not allowed to exceed 50 pixels (about 25''). We estimated fluxes for the 0.3-8 keV band from the spectrum of each source using *Sherpa* and assuming two standard models: a 5 keV thermal bremsstrahlung model with photoelectric absorption and a power-law with photon index of 1.5 and photoelectric absorption. In both cases, the  $n(H)$  was fixed at the Galactic value. Since most of the sources do not have enough counts for spectral analysis, all model parameters were frozen except for the normalizations. The 0.3-8 keV fluxes were used to calculate luminosities, using distances from the Nearby Galaxies Catalog (Tully 1988) which assumes  $H_0 = 75$  km s $^{-1}$  Mpc $^{-1}$  coupled with a Virgo infall model. Below, we present results using the thermal bremsstrahlung model; however, the results are essentially unchanged if the power-law model is used. A more detailed description of the data analysis, discussing the relevant biases and presenting source lists with spectral and timing results will be presented in a future publication (Kilgard et al., in preparation).

### 3. LUMINOSITY FUNCTIONS OF SPIRAL AND STAR FORMING GALAXIES

The cumulative luminosity functions for all galaxies are shown in Figure 1. In order to avoid incompleteness, we consider only the high luminosity range of the luminosity functions. For the nearest galaxies in our sample, we set an overall conservative completeness limit at the luminosity corresponding to a detection limit of 10 counts for NGC 1291,  $L > 3 \times 10^{37}$  erg s $^{-1}$ . In the case of the Antennae, this detection limit translates to  $L > 9 \times 10^{37}$  erg s $^{-1}$ . We derived power-law fits to the high luminosity range of the unbinned differential luminosity function using a maximum likelihood statistic following Crawford et al. (1970). The slopes range between 0.50 and 1.30; the fitted slopes,  $\gamma$ , are shown in Table 1. We evaluated the goodness of fit using a binned differential luminosity distribution and calculating the  $\chi^2$  statistic with errors computed following Gehrels (1986). The reduced  $\chi^2$  is between 0.2 and 1.0 for all galaxies except M83, which has a value of 1.6. M83 shows evidence for a break in the LF at  $\sim 9 \times 10^{37}$  ergs s $^{-1}$ .

We therefore refit the power-law including only data above this break and use this value in Table 1. The reduced  $\chi^2$  for the new fit is 0.96, indicating that a single power-law is an adequate model in this luminosity range.

Since the objects in our sample extend over large areas, the effect of interlopers in the LFs may be important. In order to assess this effect, we estimated the distribution of background sources using the logN-logS relation of Giacconi et al. (2001). Scaling the function according to the exposure time for each of our observations, we modeled the luminosity distribution of the sources with a power-law. We used this component as background for our LFs and we performed the fits again. There was little difference (less than  $1\sigma$ ) in the results of these fits and those presented above.

The early-type spiral NGC 1291 has been studied in detail by Irwin et al. (2001), who considered only bulge sources and found no sources above  $L = 2.5 \times 10^{38}$  ergs s $^{-1}$ . We include all sources in the galaxy within the S3 chip (which covers  $>80\%$  of the total area of the galaxy), which adds some higher luminosity sources. It is possible that in NGC 1291 we are seeing two populations (bulge and disk) with the disk sources becoming more prominent at higher luminosities. However, there are only 2 disk sources brighter than  $L > 3 \times 10^{38}$  ergs s $^{-1}$ , so this suggestion must be treated with caution. Finally, we note that the LF of NGC 3184 may hint at a cut-off at  $\sim 1.7 \times 10^{38}$  ergs s $^{-1}$ , with a couple of higher luminosity sources skewing the high end of the fit, but the statistics are limited. A detailed study of the LF of the Antennae has been presented in Zezas and Fabbiano (2001). The parameters of the LF they derive are very similar to those presented here. Also, a study of the LF of M82 has been presented in Zezas et al. (2001). Their slope, although somewhat flatter is consistent with our results.

The most striking feature of the results in Fig. 1 and Table 1 is that the three starburst galaxies (NGC 253, M82 and NGC 4038/9) have flatter luminosity distributions than do the spirals. This implies that the starbursts have a larger fraction of higher luminosity sources relative to the total than do the spirals. This can most naturally be explained if systems with ongoing star formation have a population of X-ray binaries that dominate the high end of the luminosity function. Due to the short time scales of the starbursts, 10-100 Myr, the high luminosity sources are most likely high-mass X-ray binaries, as the latency period for HMXBs becoming X-ray luminous is much shorter than for LMXBs. The hypothesis that the LF slope is related to star formation rate is supported by the plot in Figure 2, which shows the slopes of the luminosity functions of the galaxies discussed here plotted against the integrated 60  $\mu$ m luminosity from the IRAS faint source catalog (Moshir et al. 1992). There is a clear correlation (above the 99% confidence level) between the 60  $\mu$ m luminosity – a measure of the star formation rate (Kennicutt 1998) – and the slope of the X-ray luminosity function, in the sense that flatter slopes have higher star formation rates. The outlier is M83, which has a steep slope (deficit of high luminosity sources) relative to its 60  $\mu$ m luminosity. It is worth noting that there are several bright sources within  $D_{25}$  but off the S3 chip which may well be associated with M83. The slope is therefore an upper limit.

### 4. COMPARISON WITH RESULTS FROM LITERATURE

These results can be compared to studies of early-type systems in the literature, which are summarized in table 2. The elliptical galaxy NGC 4697 has been studied by Sarazin et al.

(2000), the S0 galaxy NGC 1553 by Blanton et al. (2001), and the bulge of M31 by Shirey et al. (2001). The luminosity distributions for NGC 4697, NGC 1553, and the bulge of M31 are not adequately described by single power-laws, but instead require broken power-laws. The exponents for the high luminosity parts of the cumulative distributions are  $\gamma = 1.79 \pm 0.26$  for M31 (Shirey et al. 2001; Primini et al. 1993),  $\gamma = 1.76^{+1.81}_{-0.39}$  for NGC 4697 (Sarazin et al. 2000), and  $\gamma = 1.7^{+0.7}_{-0.4}$  for NGC 1553 (Blanton et al. 2001). For all three galaxies, the exponent is consistent with the range  $\gamma = 1.5 - 2.1$ , steeper than the spirals and starbursts discussed above. This suggests that the trend of steeper slopes correlating with less star formation extends to early-type spirals and ellipticals. Two of these galaxies (NGC 4697 and NGC 1553) are of comparable distance to the Antennae and therefore confusion is potentially a problem. The effect of confusion on the luminosity function is complicated and depends on the clustering and luminosity properties of the sources. While a complete analysis of the effects of confusion is beyond the scope of this paper, we note that a similarly steep slope is observed in the bulge of M31 (Shirey et al. 2001; Primini et al. 1993), lending support to the hypothesis that early type systems have steeper luminosity functions.

## 5. MODEL LUMINOSITY DISTRIBUTIONS

As a first step in understanding the luminosity distributions, we adopt a simple model in which all of the X-ray sources are members of a single population with uniform properties except for luminosity and lifetime. Our goal is to show that this simple model provides an adequate framework for understanding the difference in luminosity function slopes between the various types of galaxies and the breaks in the luminosity functions of individual galaxies. More detailed modeling involving the distinctions between high-mass and low-mass X-ray binaries, and potentially including a distinct source class for the ultraluminous sources, should be done in the future. However, the basic results concerning the luminosity function derived here will remain true for each individual population of X-ray binaries in a more complex model.

The number of X-ray point sources is described at each instant in time,  $t$ , by the number of sources,  $n(t, L, T)$ , of luminosity,  $L$ , and of age,  $T$ . The source birth rate is specified by a function  $b(L, t)$  which is, in general, time dependent. The death rate should be proportional to the number of sources with the constant of proportionality given by a function  $f(L, T)$  which depends on the source properties, but not explicitly on time. In general, the evolution of sources after birth may include luminosity evolution as well as a luminosity dependent lifetime. For simplicity, we assume that each source has a constant luminosity through its lifetime. The time evolution of  $n$  is then

$$\frac{d}{dt}n(t, L, T) = b(L, t)\delta(T) - f(L, T)n(t, L, T) \quad (1)$$

where the Dirac delta function  $\delta(T)$  enforces the condition that sources are born with zero age.

The function  $f(L, T)$  determines the shape of the source lifetime distribution. We choose  $f = \delta(T - \tau(L))$ . In this case, each source of luminosity  $L$  lives a time  $\tau(L)$  and then promptly dies. To specify the lifetime  $\tau(L)$ , we note that the lifetime of an X-ray binary is determined by the time required to accrete the companion star onto the compact object. Since the luminosity is proportional to the accretion rate,  $L = \eta \dot{M} c^2$  where  $\eta \sim 0.1 - 0.4$  is the efficiency for conversion of accreted matter to luminosity,

the lifetime will depend on the luminosity as  $\tau = \eta \bar{M}_2 c^2 / \epsilon L$ , where  $\bar{M}_2$  is the average mass of the companion stars and  $\epsilon$  is the duty cycle of emission (King et al. 2001). We assume that  $\bar{M}_2$  and  $\epsilon$  are the same for all members of the population.

We note that Wu (2001) presented a model in which the source population is described only by the number of sources as a function of  $L$  and  $t$ ,  $n(t, L)$ , i.e. no information is retained concerning the age of the sources. This is equivalent to choosing a constant for the function  $f$  in our model. This choice leads to a source lifetime distribution which is a decaying exponential. Such a lifetime distribution has a great spread in ages at fixed luminosity, with many sources dying immediately after birth and some having extremely long lifetimes. Our more general model allows a narrower lifetime distribution.

We assume a power-law form for the birth rate distribution,  $b(L) \propto L^{-\alpha}$ . The power-law form is purely empirical, and provides an adequate fit to the data as discussed below. Further, we assume that the binaries turn on in X-rays instantaneously after they are formed.

If the star formation is dominated by a recent impulsive event, then the cumulative luminosity distribution shortly after the burst will be determined by the birth rate distribution,

$$N(> L) \propto L^{1-\alpha}. \quad (2)$$

If the population is allowed to evolve with no subsequent X-ray binary formation, then the high end of the luminosity distribution will be truncated as the highest luminosity sources, with the shortest lifetimes, die. The sharpness of the cutoff is determined by the sharpness of the age distribution. With the form chosen above for  $f$ , the luminosity cutoff will be extremely sharp. More realistic age distributions would produce more gradual cutoffs. Due to the limited statistics available in constraining such cutoffs, we expect that our choice for the age distribution is adequate for present data. In this case, the differential luminosity distribution is  $n(L) \propto L^{-\alpha}$  for  $L < L_B$  and  $n(L) = 0$  for  $L \geq L_B$ , where the break luminosity,  $L_B$ , is determined by the time since the burst,  $t_B$ , as  $L_B = \eta \bar{M}_2 c^2 / \epsilon t_B$ . The cumulative luminosity distribution is

$$N(> L) \propto \left(\frac{L}{L_B}\right)^{1-\alpha} - 1 \quad \text{for } L < L_B \\ N(> L) = 0 \quad \text{for } L \geq L_B \quad (3)$$

Now consider the case of gradual and long-term star formation, leading to an equilibrium between X-ray binary formation and death. If the lifetimes of the longest lived members of the X-ray point source population are significantly shorter than interval over which star formation has been proceeding steadily, then equilibrium will have been reached. The death rate at a given  $L$  will be proportional to the number of sources divided by the lifetime  $\tau(L)$  and must equal the birth rate. Since  $\tau$  is inversely proportional to  $L$  (King et al. 2001), the equilibrium luminosity distribution must be proportional to the birth rate distribution divided by  $L$ . The cumulative luminosity distribution is then

$$N(> L) \propto L^{-\alpha}. \quad (4)$$

This luminosity distribution is steeper than that of the impulsive case with an exponent that differs by one due to the (inverse) linear dependence of lifetime on luminosity.

At sufficiently low luminosities, the source lifetimes will be longer than the interval over which star formation has been proceeding steadily  $t_S$ . In general, the luminosity function will

have the form of Eq. 2 for source luminosities corresponding to source lifetimes longer than  $t_B$  and the form of Eq. 4 for higher luminosities. This leads to a broken power-law form for the luminosity distribution with the break luminosity,  $L_S$ , determined by the time since the burst,  $t_S$ , with the same relation as between  $L_B$  and  $t_B$ . The differential distribution below the break will have the same slope as that of the birth distribution, while above the slope will be steeper by one. The cumulative luminosity distribution is then

$$N(>L) = \frac{N_0 L_S}{\alpha-1} \left[ \left( \frac{L}{L_S} \right)^{1-\alpha} - 1 \right] + \frac{N_0 L_S}{\alpha} \quad \text{for } L < L_S \quad (5)$$

$$N(>L) = \frac{N_0 L_S}{\alpha} \left( \frac{L}{L_S} \right)^{-\alpha} \quad \text{for } L \geq L_S$$

where  $N_0$  is the normalization of the different luminosity distribution at  $L_S$ . Plots of this distribution for several values of  $t_S$  are shown in Fig. 3. The older systems have a steep slope in the high luminosity range. The younger systems, analogous to the starbursts, have a flatter slope over the same luminosity range and distributions extending to higher luminosities. The break luminosity depends on the duration over which X-ray binary formation has been occurring.

If X-ray binary formation proceeds continuously for some interval and then shuts off, the resulting distribution will be sharply truncated at high luminosities with the cutoff luminosity determined by the time since the shut off of X-ray binary formation. If the duration of the continuous formation interval is longer than the time since the shut off of formation, then the (differential) distribution will consist of two power-laws and a sharp high luminosity cutoff. If the opposite situation holds, the luminosity distribution will be as in Eq. 3.

As noted above, we have assumed that all of the X-ray sources are members of a single population with uniform properties except for luminosity and lifetime. In reality two types of X-ray binaries are known, low-mass and high-mass systems, which have different evolutionary paths. High-mass X-ray binaries (HMXBs) are the progeny of rapidly evolving high mass stars, while low-mass X-ray binaries (LMXBs) are descendants of slowly evolving low mass stars leading to a long latency period between star formation and the turn on in X-rays of the binaries. In the impulsive star formation case described above, the long latency of the LMXBs precludes any significant contribution from LMXBs to the luminosity distribution. Hence, the X-ray sources in starbursts are likely HMXBs, as noted above. There is also likely to be some delay between the onset of star formation and the appearance of the first HMXBs, due to time required for the first stars to go supernova. However, this can be as short as few million years, so the assumption made above of instantaneous turn on of the X-ray binaries is reasonable for star formation episodes with durations in excess of 10 Myr.

Conversely, the luminosity distribution for old systems is likely to be dominated by LMXBs because of the much longer lifetimes of the low-mass companions. For the equilibrium distributions, LMXBs and HMXBs will likely have different formation rates, companion masses, and duty cycles. This would lead to different luminosity distributions for each populations, each of which taken individually would be described by the equations presented above. The observed distribution would then be the sum of the distributions for each population.

## 6. CONCLUSIONS

Recent Chandra observations show that the X-ray source luminosity distributions of the early-type galaxies are steeper than those of the starburst galaxies with an exponent that differs by approximately one. This is similar to the difference between the slopes for our models of a burst of star formation and steady-state star formation. We suggest that the luminosity distribution of the starburst galaxies directly reflects the birth luminosity distribution, while the other galaxies have a similar birth luminosity distribution and an observed luminosity distribution modified by the effects of an aging X-ray binary population. The slopes of the spirals are intermediate between the two cases, which may arise from a combination of the two components, as suggested above for NGC 1291.

For galaxies where the LF is measured over a broad luminosity range, it may be possible to detect breaks in the luminosity function and relate them to the galaxy's star formation history (Wu 2001). Shirey et al. (2001) reports a break in the LF for M31's bulge near  $3 \times 10^{37} \text{ ergs s}^{-1}$ . Applying the relation found above between the break luminosity and age of the X-ray binary population, we find  $t_B$  of the order of 10 Gyr for  $\epsilon = 0.02$ ,  $\eta = 0.1$ , and  $\bar{M}_2 = 2M_\odot$ . The difference in slope above and below the break is  $1.32 \pm 0.26$ , close to the difference of 1 predicted in our simple model. The breaks in NGC 4697 and NGC 1553 are at higher luminosities, suggesting shorter  $t_B$ . However, the break luminosities are uncertain due to the distance uncertainties. There are suggestions of breaks at even higher luminosities, above  $10^{39} \text{ ergs s}^{-1}$  in the starbursts M82 and the Antennae. In the context of the model presented above, this would be consistent with the rather short ( $\lesssim 100$  Myr) durations of the starburst events in these galaxies.

An alternate explanation of the luminosity function breaks is that they are due to the transition between neutron star and black hole X-ray binaries (Sarazin et al. 2000). This suggestion is motivated by the observation that the break luminosity in the elliptical galaxies is close to the Eddington limit of a  $1.4 M_\odot$  neutron star (Sarazin et al. 2000). However, the lower break luminosity found in M31 and the higher, although only marginally detected, break luminosities in the starbursts would argue against this interpretation. Additional X-ray luminosity function measurements are required to determine whether the break luminosity is related to the Eddington luminosity or to the star-formation history of each galaxy as suggested here.

The striking differences in the luminosity functions and the progress that can be made in understanding the distributions with a simple model indicate that X-ray point source luminosity distributions should prove to be a powerful tool in understanding the evolutionary history of massive star populations in external galaxies. New Chandra observations of a large sample of galaxies across the full Hubble sequence coupled with detailed stellar evolution models should provide new insights into the compact object populations of external galaxies.

## 7. ACKNOWLEDGEMENTS

We thank the CXC DS and SDS teams for providing the software used in analysis and Harvey Tananbaum and Vinay Kashyap for valuable comments on the text and discussions. This work was partially supported by NASA contract NAS 8-39073 (CXC) and grant GO1-2092A. PK acknowledges partial support from NASA grant NAG5-7405.

## REFERENCES

Alton, P.B., Trehewella, M., Davies, J.I., Evans, R., Bianchi, S., Gear, W., Thronson, H., Valentijn, E., Witt, A. 1998, A&A, 335, 807

Blanton, E.L., Sarazin, C.L., & Irwin, J.A. 2001, ApJ, 552, 106

Cash, W. 1979, ApJ, 228, 939

Crawford, D.F., Jauncey, D.L., & Murdoch, H.S. 1970, ApJ, 162, 405

Fabbiano, G. 1989, ARA&A, 27, 87

Fabbiano, G., Zezas, A., & Murray, S.S. 2001, ApJ, 554, 1035

Freeman, P.E., Kashyap, V., Rosner, R., & Lamb, D.Q. 2002, ApJS, in press

Garcia, M.R., Murray, S.S., Primini, F.A., Forman, W.R., McClintock, J.E., & Jones, C. 2000, ApJ, 537, 23

Gehrels, N. 1986, ApJ, 303, 336

Giacconi, R., Rosati, P., Tozzi, P., Nonino, M., Hasinger, G., Norman, C., Bergeron, J., Borgani, S., Gilli, R., Gilmozzi, R., & Zheng, W. 2001, ApJ, 551, 624

Helou, G., Soifer, B.T., Rowan-Robinson, M. 1985, ApJ, 298, 7

Irwin, J.A., Sarazin, C.L., & Bregman, J.N. 2001, ApJ, submitted

Kennicutt, R.C. 1998, ARA&A, 36, 189

King, A.R., Davies, M.B., Ward, M.J., Fabbiano, G., & Elvis, M. 2001, ApJ, 552, 109

Lira, P., Ward, M., Zezas A., Alonso-Herrero A., & Ueno S. 2001, MNRAS, in press (astro-ph/0109198)

Long, K.S., Charles, P.A., Blair, W.P., & Gordon, S.M. 1996, ApJ, 466, 750

Moshir, M., Kopan, G., Conrow, J. et al. 1992, Explanatory Supplement to the IRAS Faint Source Survey, Version 2, JPL D-10015 8/92. Jet Prop. Lab., Pasadena, Calif.

Primini, F.A., Forman, W., and Jones, C. 1993, ApJ, 410, 615

Rice, W., Lonsdale, C.J., Soifer, B.T., Neugebauer, G., Kopan, E.L., Lloyd, L.A., de Jong, T., and Habing, H.J. 1988, ApJS, 68 91.

Rieke, G.H. & Lebofsky, M.J. 1978, ApJ, 220, 37.

Sarazin, C.L., Irwin, J.A., and Bregman, J.N. 2000, ApJ, 544, 101

Shirey, R., Soria, R., Borozdin, K., Osborne, J.P., Tiengo, A., Guainazzi, M., Hayter, C., La Palombara, N., Mason, K., Molendi, S., Paerels, F., Pietsch, W., Priedhorsky, W., Read, A.M., Watson, M.G., & West, R.G. 2001, A&A, 365, 195

Soria, R. & Wu, K. 2002, A&A, accepted

Strickland, D.K., Heckman, T.M., Weaver, K.A., & Dahlem, M. 2000, AJ, 120, 2965

Telesco, C.M., Dressel, L.L., and Woltscroft, R.D. 1993, ApJ, 414, 120

Tully, R.B. 1988, Nearby Galaxies Catalog, Cambridge University Press (Cambridge).

Wu, K. 2001, Publ. Astron. Soc. Australia, accepted

Zezas, A., Fabbiano, G., Prestwich, A., Ward, M., & Murray, S. 2001, in "The Central kpc of Starburst and AGN", APS Conf. Series 249, 425, Eds. J.H. Knapen, J.E. Beckman, I. Shlosman, and T.J. Mahoney

Zezas, A. & Fabbiano, G. 2001, ApJ, submitted

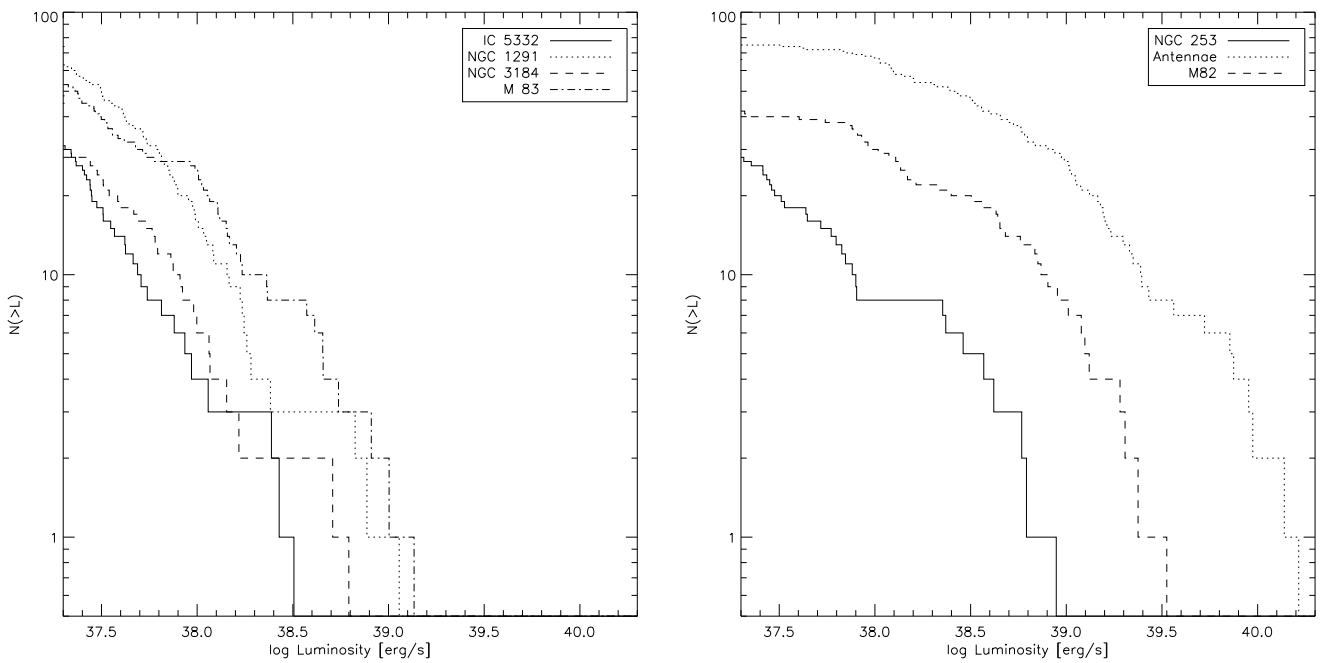


FIG. 1.— Cumulative Luminosity functions of spirals (left) and starbursts (right).

TABLE 1  
PROPERTIES OF OBSERVATIONS AND GALAXIES

Galaxy	Hubble type	ObsID	Date	Exposure (sec)	$n_{\text{H}}$ ( $10^{20}$ cm)	$D_{25}$ fraction	Distance (Mpc)	LF Slope	60 $\mu\text{m}$ luminosity ( $10^{40}$ erg/s)
NGC 1291	S0/a	795	2000-06-27	37637	2.24	0.78	8.6	$1.07 \pm 0.15$	8.77
M83	Sc	793	2000-04-29	48562	3.70	0.73	4.7	$1.38 \pm 0.28$	127
NGC 3184	Scd	1520	2000-01-08	38419	1.15	1.0	8.7	$1.11 \pm 0.22$	29.6
IC 5332	Sd	2066	2001-05-02	51986	1.38	0.81	8.4	$1.30 \pm 0.31$	6.09
M 82	I0	361	1999-09-20	32710	4.03	0.81	5.2	$0.50 \pm 0.08$	1370
NGC 253	SAB	969	1999-12-16	12207	1.43	0.45	3.0	$0.81 \pm 0.15$	324
Antennae	SA/SB(pec)	315	1999-12-01	70813	3.95	0.85	25.5	$0.53 \pm 0.07$	1350

TABLE 2  
LF SLOPE AND 60  $\mu$ M LUMINOSITY OF EARLY-TYPE GALAXIES

Galaxy	Hubble type	LF Slope	60 $\mu$ m luminosity ( $10^{40}$ erg/s)	Reference
NGC 1553	S0	$1.7^{+0.7}_{-0.4}$	37.7	Blanton et al. (2001)
NGC 4697	E6	$1.76^{+1.81}_{-0.39}$	59.5	Sarazin et al. (2000)
M31 (bulge)	Sb	$1.79 \pm 0.26$	102	(Shirey et al. 2001; Primini et al. 1993)

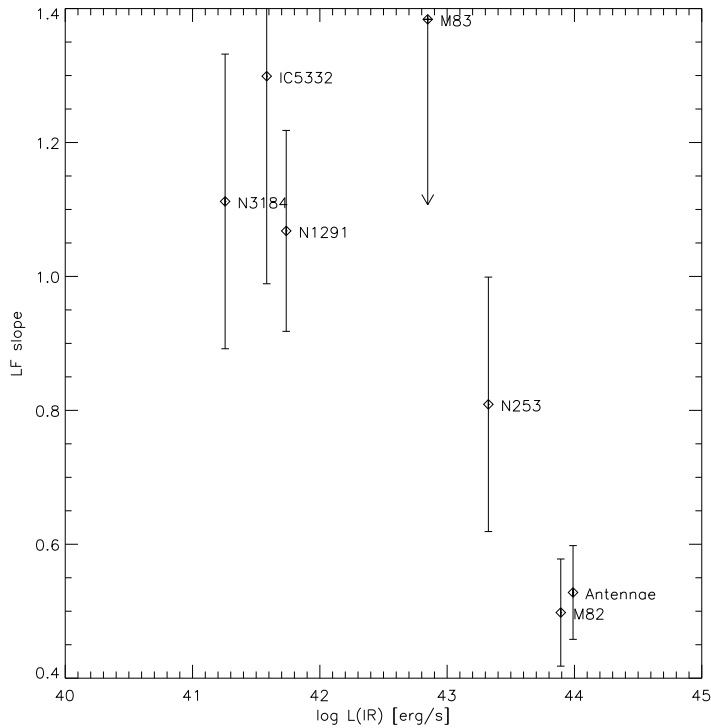


FIG. 2.— Cumulative luminosity function slope vs. 60  $\mu$ m luminosity.

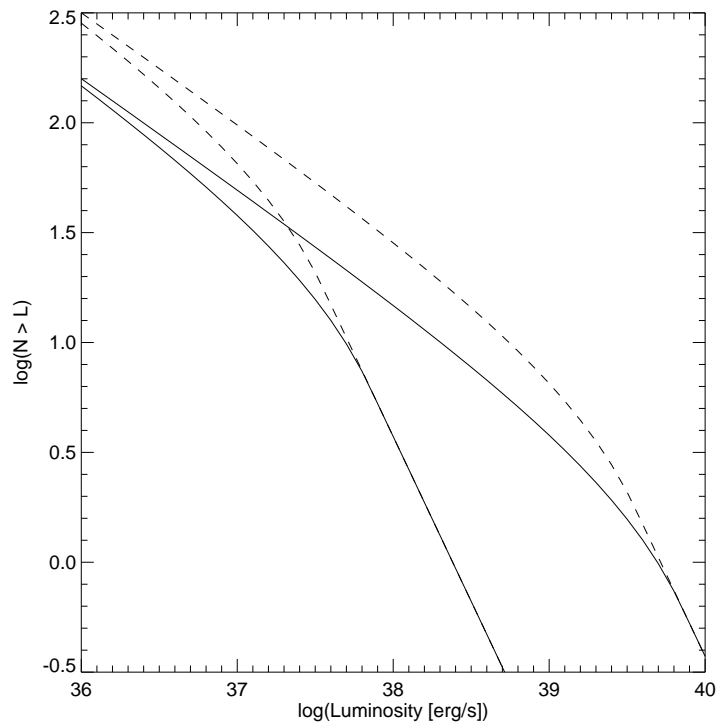


FIG. 3.— Model cumulative luminosity functions. The upper two curves are continuous star formation for 10 Myr (solid) and 20 Myr (dashed). The lower curves are for 1 Gyr (solid) and 2 Gyr (dashed) with a star formation rate lower by a factor of 100.